ChemPubSoc Europe

DOI: 10.1002/chem.201705957

CHEMISTRY A European Journal Full Paper

Redox Chemistry | *Hot Paper*

Ligand- and Metal-Based Reactivity of a Neutral Ruthenium Diolefin Diazadiene Complex: The Innocent, the Guilty and the Suspicious

Vivek Sinha,[a] Bruno Pribanic,[b] Bas de Bruin,*[a] Monica Trincado,*[b] and Hansjörg Grützmacher*[b]

In memory of Professor José Barluenga

Abstract: Coordination of the diazadiene diolefin ligand ($trop_2dad$) to ruthenium leads to various complexes of composition [Ru($trop_2dad$)(L)]. DFT studies indicate that the closed-shell singlet (CSS), open-shell singlet (OSS), and triplet electronic structures of this species are close in energy, with the OSS spin configuration being the lowest in energy for all tested functionals. Singlet-state CASSCF calculations revealed a significant multireference character for these complexes. The closed-shell singlet wavefunction dominates, but these complexes have a significant (≈8–16%) open-shell singlet [d^7-Ru^I(L)($trop_2dad^{\bullet-}$)] contribution mixed into the ground state. In agreement with their ambivalent electronic structure, these complexes reveal both metal- and ligand-centered reactivity. Most notable are the reactions with AdN_3, diazomethane, and a phosphaalkyne leading to scission of the C–C bond of the diazadiene (dad) moiety of the $trop_2dad$ ligand, resulting in net (formal) nitrene, carbene, or P≡C insertion in the dad C–C bond, respectively. Supporting DFT studies revealed that several of the ligand-based reactions proceed via low-barrier radical-type pathways, involving the $dad^{\bullet-}$ ligand radical character of the OSS or triplet species.

Introduction

The concepts of cooperative[1] and redox non-innocent ligands[2] have been used in several research areas, which range from coordination chemistry to homogeneous catalysis.[3] In biology, ligand radicals (amino acid or porphyrin) bound to transition metals play a crucial role in the mechanism of a variety of relevant biosynthetic and metabolic processes mediated by metalloenzymes (e.g., galactose oxidase, cytochrome P450, methane monooxygenase).[4] The synthetic accessibility to metal complexes with reactive radical ligands has allowed chemists to tackle challenging catalytic processes (alcohol and methane oxidation, N_2 fixation, water splitting).[5] Compared to closed-shell complexes, non-innocent radical ligands with discrete or considerable spin density on the organic fragment alter the reactivity profile of a complex considerably.[3] The cooperativity between the metal center and the coordinated radical in M–L$^{\bullet}$ allows selective transformations avoiding the uncontrolled reactivity archetypal of free radicals. α-Diimines (diazadienes = dad) are classical examples of redox non-innocent ligands.[2d,6] Single-electron transfer steps (using external reducing agents or directly from the metal) to the dad ligand convert the neutral closed-shell diimine $M^n(L^0)$ into the open-shell π-radical anion ligand species $M^{n+1}(L^{\bullet-})$, and further to the closed-shell dianionic bisamido ligand complexes $M^{n+2}(L^{2-})$ (Scheme 1, top).[7] The π-electron system in the α-diimine-backbone in combination with two π-accepting olefins in the chelating tetradentate $trop_2dad$ ligand, which stabilizes metal centers in low oxidation states, allows for the formulation of distinct redox-isomeric mesomeric structures. Depending on the nature of the metal ion and the extent of the (parallel or antiparallel) metal–ligand spin coupling, these electromers can also exist in different spin configurations, which could well play a key role in the ensuing reactivity.[8]

We previously synthesized the ruthenium complex [$K(dme)_2$][Ru(H)($trop_2dad$)] [$trop_2dad$ = 1,4-bis(5*H*-dibenzo[*a*,*d*]cyclohepten-5-yl)-1,4-diazabuta-1,3-diene], which catalyzes the methanol[9] and formaldehyde[10] reforming to CO_2 and H_2

[a] *V. Sinha, Prof. Dr. B. de Bruin*
Supramolecular and Homogeneous Catalysis Group
Van't Hoff Institute for Molecular Sciences (HIMS)
University of Amsterdam, Science park 904
1098XH, Amsterdam (The Netherlands)
E-mail: b.debruin@uva.nl

[b] *B. Pribanic, Dr. M. Trincado, Prof. Dr. H. Grützmacher*
Department of Chemistry and Applied Biosciences ETH Zürich
Laboratory of Inorganic Chemistry, Vladimir-Prelog-Weg 1
Zürich CH-8093 (Switzerland)
E-mail: trincado@inorg.chem.ethz.ch
hgruetzmacher@ethz.ch

Supporting information and the ORCID identification numbers for the authors of this article can be found under: https://doi.org/10.1002/chem.201705957.

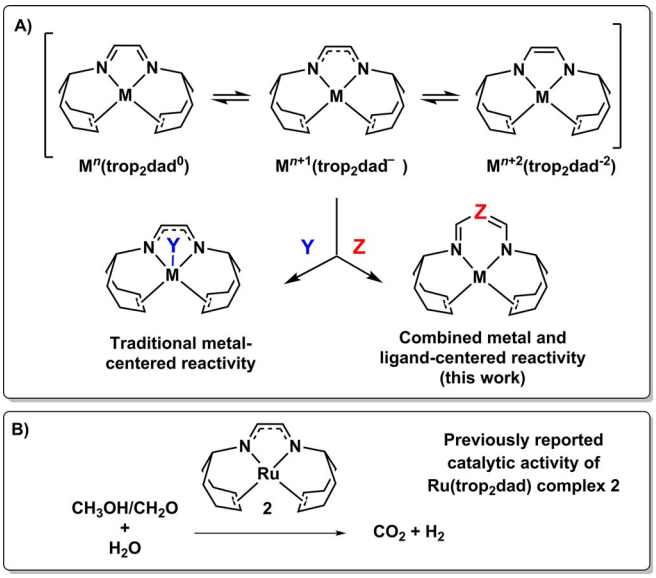

Scheme 1. A) Possible valence isomers of a non-innocent dad-diolefin metal complex, giving rise to both metal- and ligand-centered reactivity. B) Reported activity of ruthenium trop$_2$dad complex **2** in catalytic dehydrogenation of aqueous methanol or formaldehyde mixtures.

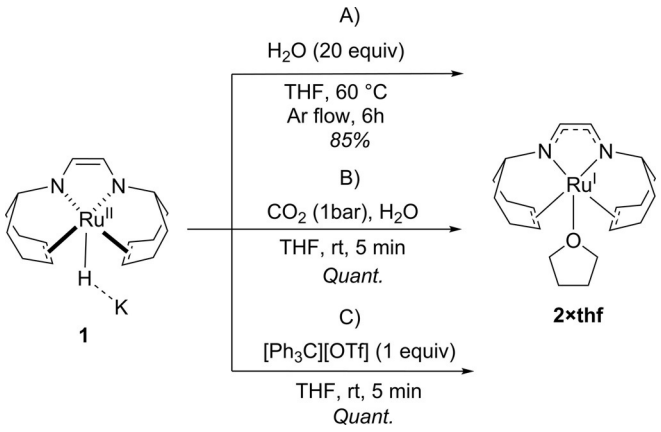

Scheme 2. Synthesis of complex **2×thf** by protonation of **1** under neutral conditions (method A), mild acidic conditions (method B), or by hydride abstraction by a trityl reagent (method C).

(Scheme 1 B). In the reaction, water is used as the sole "oxidant"—that is, it serves as the oxygenating agent—and the methanol dehydrogenation process occurs without additives. The mechanism proposed for this reaction involves the initial formation of the neutral species [Ru(trop$_2$dad)] (**2**) formed by protonation of the hydrido ruthenate complex **1**, followed by hydrogen transfer from the substrate to the "chemically cooperative" 1,4-diazabutadiene converting the ligand backbone to the diamine form.

Herein, we report the synthesis and characterization of the neutral species **2×thf**. DFT and CASSCF calculations were used to investigate the redox-active nature of the ligand. Further reactivity studies of **2×thf** with a series of substrates (organoazide, diazomethane, nitrosoalkane, phosphaalkyne, and a metal carbonyl) were carried out. The reactivity pattern is notable, and it was found to be ligand centered, metal centered, or both, depending on the substrate (Scheme 1, bottom). Supporting computational studies suggest that the redox non-innocence of the dad ligand plays an important role in several of the remarkable transformations described herein.

Results and Discussion

Synthesis of [Ru(trop$_2$dad)L] and its electronic structure

Complex [Ru(trop$_2$dad)] (**2**) was initially prepared by the reaction of complex **1** with an excess of H_2O in THF at 60 °C. Under these conditions, the reaction requires a few hours to complete. The process can be considerably accelerated, if the reaction is performed under a CO_2 atmosphere in the presence of stoichiometric amounts of water. Alternatively, the hydride ligand can be rapidly abstracted with the trityl salt [Ph_3C][OTf]. The last two reactions occur instantly (< 5 min) at room temperature, giving **2** as the solely spectroscopically detected species in solution (Scheme 2). The observation of only single resonances for the olefinic groups and the imine protons in the ^{1}H NMR spectrum is consistent with an (averaged on the NMR time scale) C_{2v} symmetry in solution. The ^{13}C NMR spectrum shows the "imine carbons" of the complex **2** at $\delta = 147.5$ ppm and the four equivalent olefinic carbons at $\delta = 72.2$ ppm, considerably shifted to higher frequencies with respect to the pentacoordinate divalent ruthenium precursor **1** (125.8 ppm for N–C and 66.5–52.8 ppm for C=C$_{trop}$).

The corresponding adduct **2×thf** could be isolated as dark red single crystals and was characterized structurally by X-ray diffraction methods (Figure 1). The metal center resides in a square pyramidal geometry ($\tau_5 = 0.1$) with the two imine N atoms and two olefins in the basal position ($\alpha \approx \beta = 155.0/160.9°$). The O-bound THF molecule occupies the apical position.[11] The average C=C$_{trop}$ (1.436(3) Å) and Ru-ct (ct = centroid of C=C$_{trop}$) bond lengths (2.039(2) Å) indicate efficient electron donation from the metal into the π^* orbitals of the coordinat-

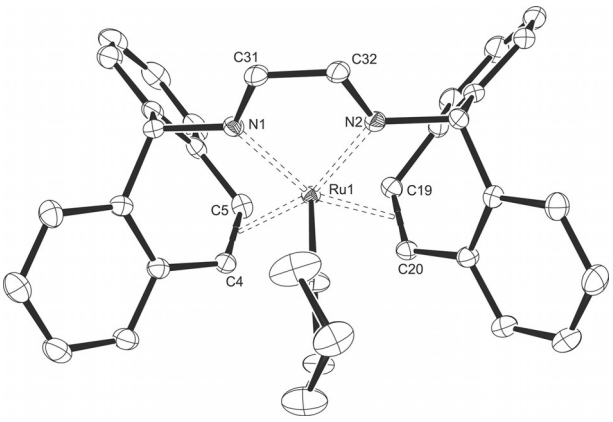

Figure 1. ORTEP plot of **2×thf** at 50% ellipsoid probability. Hydrogen atoms are omitted for clarity. Selected bond lengths [Å] and angles [°]: Ru1–ct1 2.041(2), Ru1–ct2 2.039(2), C4–C5 1.431(3), C19–C20 1.443(3), Ru1–N1 2.000(2), Ru1–N2 2.006(2), N1–C31 1.335(3), N2–C32 1.337(3), C31–C32 1.405(3); ct1-Ru1-ct2 100.75(8), ct1-Ru1-N1 88.01(7), ct2-Ru1-N2 87.32(7), N1-Ru1-N2 77.98(7).

ed olefin groups, as was observed likewise in the hydride complex **1**. But the slightly longer Ru–N distances (2.002(2) Å versus 1.971(5) Å) and the bond lengths within the dad backbone indicate a transition from the 1,2-diamido ethylene form, [tropN-CH=CH-N-trop]$^{2-}$ in **1** with N–C 1.352(8) Å(av) and C=C 1.377(8) Å to a less-reduced form in **2×tfh** with N–C_{av} 1.335(3) Å(av) and C–C 1.404(3) Å. These values are close to those previously reported for the analogous five-coordinated diolefin-diazadiene Fe complexes [Fe(trop$_2$dad)(L)] (L = THF, ACN, PPh_3) (N–C_{av} 1.327(5) Å; C=C_{av} 1.393(5) Å), which are best described as species containing a monoanionic radical ligand (dad)$^{\bullet-}$ coordinated to Fe^{I}.[12] Another recent example is the complex [Fe(trop$_2$dad)$_2$], which contains a high-spin Fe^{II} center with two N′N′-coordinated monoanionic radical ligands.[13] Magnetic susceptibility measurements were performed for **2×tfh** in the solid state in the temperature range of 2–300 K and indicate a diamagnetic compound. A solution of **2×thf** in THF is EPR silent at 298 and at 110 K. Therefore, the experimental results suggest that **2×thf** can be described as a Ru^{I} complex containing a monoanionic radical ligand with antiparallel electron spins leading to a diamagnetic ground state ($S=0$). Alternatively, the molecule could be described as a ruthenium(0) complex with substantial π-back donation into the π*-system of the neutral dad moiety of the trop$_2$dad ligand (net ~one-electron transfer).

We performed DFT calculations on full atom models of the four-coordinate square planar complex [Ru(trop$_2$dad)] (**2**), the five-coordinate square pyramidal water complex [Ru(trop$_2$dad)(OH_2)] (**2×H_2O**), and the THF adduct [Ru(trop$_2$dad)(thf)] (**2×thf**) in three different DFT electronic configurations: 1) closed-shell singlet ($S=0$; spin-restricted singlet); 2) open-shell singlet ($S=0$; spin-unrestricted singlet, broken symmetry approach); and 3) triplet ($S=2$; spin unrestricted; Table 1).[14a]

Table 1. DFT computed relative energies [kcal mol^{-1}] of the [Ru(trop$_2$dad)(L)] species **2**, **2×H_2O**, and **2×thf** in three different electronic-structure configurations.

Species Complex **2**	$<S^2>$ [a]	Δ(SCF + ZPE) [b]	ΔH_{rel} [c]	ΔG_{rel} [d]
^{1}**2**$_{CSS}$	0.0	+4.0	+4.0	+4.0
^{1}**2**$_{OSS}$	0.62	0	0	0
^{3}**2**	2.01	+10.2	+10.4	+9.9
Complex **2×thf**				
^{1}**2×thf**$_{CSS}$	0.0	+3.3	+3.3	+2.8
^{1}**2×thf**$_{OSS}$	0.25	0	0	0
^{3}**2×thf**	2.01	+6.9	+7.2	+6.4
Complex **2×H_2O**				
^{1}**2×H_2O**$_{CSS}$	0.0	+3.9	+3.7	+4.2
^{1}**2×H_2O**$_{OSS}$	0.37	0.0	0.0	0.0
^{3}**2×H_2O**	2.01	+6.2	+6.8	+4.8

[a] Expectation value of the total spin operation. [b] Relative zero-point energy corrected SCF energy, for singlet-biradical configurations the SCF energy has been corrected for triplet contamination (see the Supporting Information for details). [c] Relative enthalpy. [d] Relative Gibbs free energy.

The closed-shell singlet (CSS) configurations of all complexes are best described with equal contributions of two resonance structures, Ru^0(dad^0) and Ru^{II}(dad^{2-}). The first contains a neutral, low-spin d^8 ruthenium(0) center supported by a neutral trop$_2$dad ligand and the second a dicationic, low-spin d^6 ruthenium(+II) center supported by a dianionic trop$_2$dad^{2-} ligand. These electronic structures reflect metal-to-ligand π-back donation and ligand-to-metal π-donation models. Both the triplet and the open-shell singlet configurations are best described as metallo-radical-ligand radical Ru^{I}(trop$_2$dad$<$MI$>^{-}$) species, each containing a mono-cationic, low-spin d^7 ruthenium(+I) center ($S=^1/_2$) supported by a monoanionic trop$_2$dad$^{\bullet-}$ radical-type ligand ($S=^1/_2$). They differ in the exchange-coupling interactions between the unpaired electrons centered on the metal and the ligand. In the OSS configuration the metal and ligand centered unpaired electrons have anti-parallel spins (overall $S=0$), whereas in the triplet configuration, they are parallel ($S=1$). This is reflected in the spin-density plots shown in Figure 2 for the adduct **2×H_2O** as example.

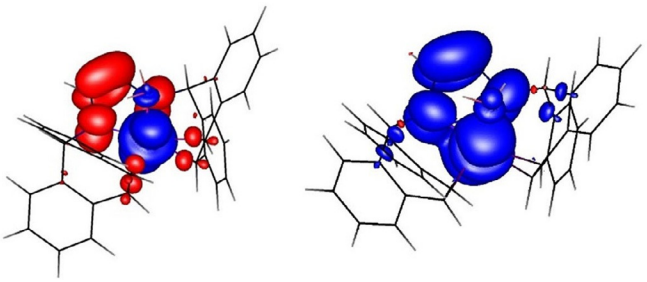

Figure 2. Spin-density plots of open-shell singlet (left) and triplet (right) configurations of **2×H_2O**.

In all cases (**2**, **2×H_2O**, and **2×thf**), the triplet electronic structure is the least stable configuration (Table 1). The OSS configuration is calculated to be the most stable in all cases. However, the energy differences are rather small. Note that in all complexes, the C–N and C–C bond lengths in the diazadiene moiety are very similar and do not allow a distinction between the three electronic configurations. But the calculated distances to the axial THF ligand in triplet **2×thf** (2.699 Å) is much longer than the experimentally observed Ru–O distance in **2×thf** (2.244 Å; see the Supporting Information for details). Therefore, we exclude a significant population of the triplet state and its participation in reactions performed with Ru(trop$_2$dad) complexes.

A reliable distinction between the open-shell singlet (singlet biradical) complexes [d^7-Ru^{I}(L)(trop$_2$dad$^{\bullet-}$)] and closed shell [d^6-Ru^{II}(L)(trop$_2$dad^{2-})]↔[d^8-Ru^0(L)(trop$_2$dad)] cannot be made on the basis of the DFT models alone.

Predicting relative energies of species in different spin configurations with DFT methods can be troublesome,[15] specifically when the relative stability of open-shell versus closed shell singlet electronic structures is concerned.[16] Therefore, we performed (singlet-state) CASSCF calculations on OSS and CSS optimized geometries of complexes **2** and **2×thf**.[14b] The

CASSCF results indicate that in both complexes the closed-shell singlet wavefunction dominates, but with a significant (≈8–16%) open-shell singlet [d^7-Ru^I(L)($trop_2dad^{\bullet-}$)] contribution mixed into the ground state (see the Supporting Information for further details). This is in agreement with the DFT results, showing similar OSS and CSS energies with a slight preference for the OSS configuration (see Table 1). It thus seems safe to conclude that **2** and **2×thf** have singlet ground states, with a significant [d^7-Ru^I(L)($trop_2dad^{\bullet-}$)] OSS character each.

We thus wondered if the OSS [d^7-Ru^I(L)($trop_2dad^{\bullet-}$)] character of these species would also have an influence on their reactivity, and therefore, we set out to seek for reactions, in which the radical character of the dad ligand could be involved (Scheme 3).

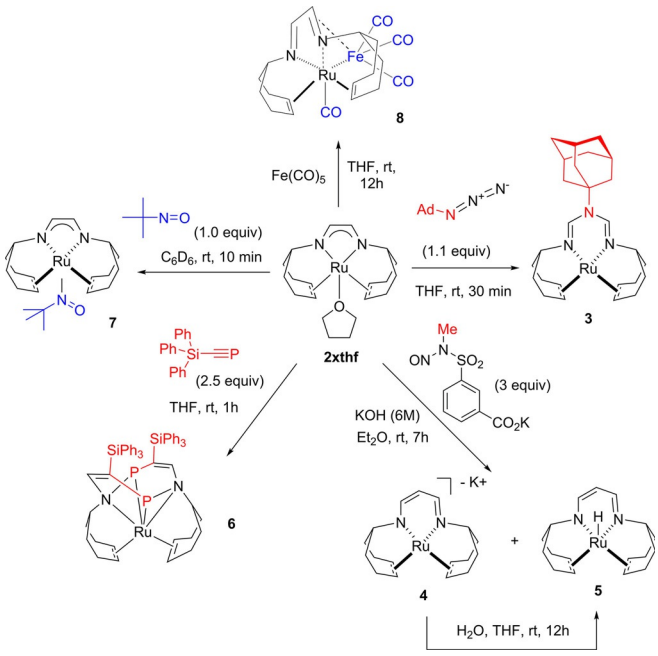

Scheme 3. Overview of ligand- and metal-centered reactivity of complex **2×thf**.

Reactivity studies of complex 2×thf

When complex **2×thf** was reacted with equimolecular amounts of an organic azide (AdN_3, Ad = adamantyl), a color change from brown to bright red occurred instantly (Scheme 3). Analysis of the reaction mixture by NMR spectroscopy showed the nearly complete conversion of complex **2×thf** to a new species, which was isolated in the form of red single crystals in good yield (84%) and characterized by X-ray structure analysis (Figure 3 A).

In the resulting complex [Ru(trop-N=C-N(Ad)-C=*N*-trop)] (**3**), an adamantyl nitrene moiety has been inserted into the C–C bond of the dad backbone leading to an aza-β-dialdimine ligand (N-nacnac). The ruthenium center in **3** is in a slightly distorted square-planar coordination environment [inter-plane angle ϕ (N1-Ru1-ct1 < N2-Ru1-ct2) 7.5°]. The averaged C31/32-N1/2 bonds (1.278(7) Å) are significantly shorter than the C31-N3/C32-N3 bonds (1.370(9) Å) and indicate that **3** is best described as a Ru^0 complex with an "innocent" tetradentate trop-N=CH-NAd-CH=N-trop ligand. In the nearly planar conformation of the ligand backbone, the lone pair on the central amine (N3) atom interacts with the two adjacent imine (p,p)π* antibonding orbitals leading to a conjugated N=C-N-C=N unit with partial double-bond character.[17] In the calculated mechanism for the nitrene insertion (see below), an imide diradical complex is invoked as transient intermediate. A related mechanism has been proposed very recently for a chromium complex, as was reported by Heins et al.[18] In an analogous manner, complex **2** is expected to cleave diazomethane, CH_2N_2, and form a methylene ligand under loss of N_2 which eventually interacts with the dad ligand and forms likewise an insertion product.[19] In a previous study, Carreira and co-workers employed a water-soluble diazomethane precursor for the metal-catalyzed cyclopropanation reaction of alkenes.[20] We used this reagent in a base-mediated tandem diazomethane generation/carbene transfer reaction to the [Ru($trop_2dad$)] complex. In a biphasic solvent mixture of water and diethylether, the potassi-

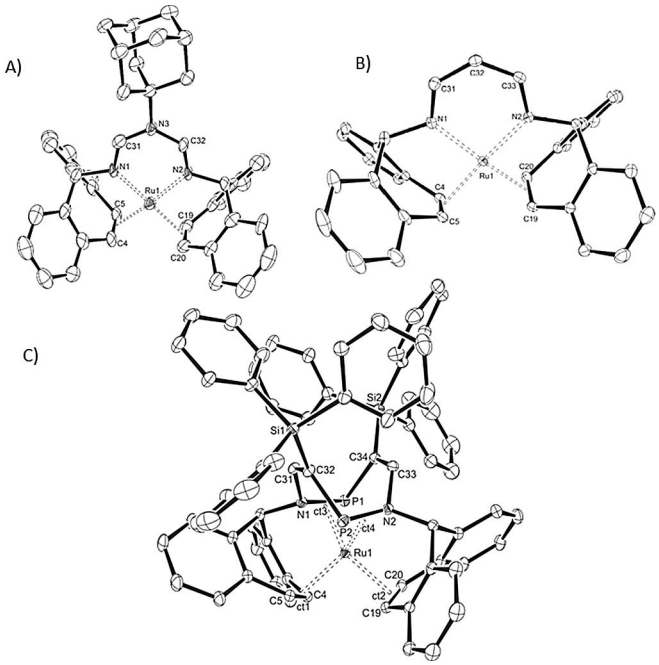

Figure 3. ORTEP plots of **3**, **4**, and **6** at 50% ellipsoid probability and selected bond lengths [Å] and angles [°]. A) Complex **3**. Hydrogen atoms and solvent molecules are omitted for clarity. Only one of the two molecules of **3** in the asymmetric unit is shown. Ru1–ct1 1.994(7), Ru1–ct2 1.995(6), C4–C5 1.427(7), C19–C20 1.420(7), Ru1–N1 2.070(4), Ru1–N2 2.082(5), N1–C31 1.276(7), N2–C32 1.279(6), C31–N3 1.363(9), C32–N3 1.377(6); ct1-Ru1-ct2 92.58(2), ct1-Ru1-N1 90.05(2), ct2-Ru1-N2 90.64(2), N1-Ru1-N2 87.2(2). B) Complex **4**. Selected hydrogen atoms, solvent molecules, and the counterion have been omitted for clarity. Ru1–N1 2.057(1), Ru1–N2 2.056(1), Ru1–ct1 1.999(2), Ru1–ct2 2.005(2), C4–C5 1.447(2), C19–C20 1.443(2), N1–C31 1.327(2), C31–C32 1.392(2), C32–C33 1.396(2), C33–N2 1.326(2); N2-Ru1-N1 90.22(5), N1-Ru1-ct1 89.41(5), N2-Ru1-ct2 89.68(5). C) Complex **6**. Selected hydrogen atoms are omitted for clarity. Ru1–ct1 2.044(1), Ru1–ct2 2.036(1), Ru1–ct3 2.037(1), Ru1–ct4 2.043(1), C4–C5 1.437(1), C19–C20 1.443(1), N1–P1 1.801(1), N2–P2 1.816(1), N1–C31 1.447(1), N2–C33 1.450(1), C31–C32 1.337(1), C33–C34 1.337(1), P1–C34 1.847(1), P2–C32 1.847(1); ct1-Ru1-ct2 96.03(3), ct1-Ru1-ct3 98.19(3), ct2-Ru1-ct4 99.00(3), ct3-Ru1-ct4 95.28(3), C34-P1-N1 96.56(3), C32-P2-N2 97.52(3), P1-N1-C31 122.86(5), P2-N2-C33 122.29(5).

um salt of the *N*-nitrososulfonamide compound is converted under basic conditions to diazomethane in situ, which is extracted continuously into the ethereal solution containing **2**. The reaction between $H_2C{=}N_2$ and **2** gives a mixture of complexes **4** and **5** in a 1:4 ratio (Scheme 2). The solid-state structure of **4** indicates an insertion of a transient carbene unit into the C–C bond of the ligand backbone, which under the reaction conditions, further rearranges and/or is deprotonated to **4** with a conjugated central metallacycle (Figure 4B). The neutral

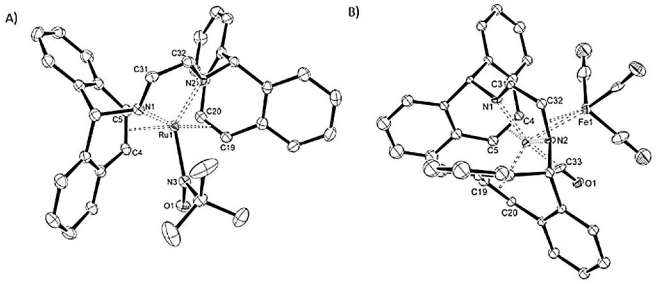

Figure 4. ORTEP plots of complex **7** and **8** at 50% ellipsoid probability. Hydrogen atoms are omitted for clarity. Selected bond lengths [Å] and angles [°]. A) Complex **7**: Ru1–ct1 2.107(3), Ru1–ct2 2.143(3), C4–C5 1.421(3), C19–C20 1.396(3), Ru1–N1 1.997(2), Ru1–N2 1.980(2), N1–C31 1.356(4), N2–C32 1.349(4), C31–C32 1.369(3), Ru1–N3 1.995(2), N3–O1 1.246(3); ct1-Ru1-ct2 99.4(1), ct1-Ru1-N1 85.31(9), ct2-Ru1-N2 86.52(9), N1-Ru1-N2 78.79(9), ct1-Ru1-N3 101.02(9), ct2-Ru1-N3 89.74(9), N1-Ru1-N3 104.49(9), N2-Ru1-N3 129.03(9). B) Complex **8**: Ru1–ct1 2.045(2), Ru1–ct2 2.241(1), C4–C5 1.42(2), C19–C20 1.41(1), Ru1–N1 2.065(7), Ru1–N2 2.06(1), Ru1–C33 1.85(1), N1–C31 1.28(2), N2–C32 1.43(1), C31–C32 1.42(2), Fe1–N2 1.875(9), Fe1–C32 2.06(1); ct1-Ru1-ct2 108.89(4), ct1-Ru1-N1 85.52(4), ct2-Ru1-N2 83.75(4), N1-Ru1-N2 81.1(4), ct1-Ru1-C33 88.36(6), ct2-Ru1-C33 93.69(5).

hydride complex **5**—obtained as major product—can be obtained by direct protonation of isolated **4** with water. The structure of **4** shows a $[Ru(tropN(CH)_3Ntrop)]^-$ anion and a $[K(dme)_2]^+$ cation, which form an electrostatically enforced host–guest complex, in which the K^+ ion interacts with one of the benzo groups of the ligand. The ruthenium center, the two N atoms, and the three CH groups in the backbone are in the same plane from which the two centroids (ct) of the coordinated olefins slightly deviate forming a very slightly distorted square-planar structure [inter-plane angle ϕ 2.2°] (Figure 3B). The ligand in **4** (and **5**) corresponds to a classical monoanionic β-dialdimanto ligand[21] with short N1(2)–C31(32) (av 1.327(2) Å) and C31–C32 and C32–C33 distances (av 1.394(2) Å) indicating a six-membered metallacycle with a delocalized π system [N=CH-CH=CH-N^-↔-N-CH=CH-CH=N].[22]

The observed insertions of a nitrene or carbene in the diazadiene unit indicate chemical "non-innocence" and prompted us to investigate the reaction of **2×thf** with a phosphaalkyne as a strong dipolaro- and dienophile (Scheme 2). The oligomerization of phosphaalkynes in the coordination sphere of transition metals has been extensively studied,[23] and new heterocyclic and cage compounds were obtained by cycloaddition reactions with a variety of unsaturated substrates.[24] We reacted the silyl phosphacyanide, $Ph_3Si–C{\equiv}P$,[25] with **2×thf**, which led to the formation of complex **6**. The unique structure of this compound was determined by single-crystal X-ray diffraction methods and is shown in Figure 3C. Two phosphaalkyne units are formally inserted into the central C–C bond of the dad unit to give an unprecedented 1,5,2,6-diazadiphosphocine heterocycle.[26] The central eight-membered heterocycle adopts a boat conformation and can be seen as a heteroatom analogue of cyclooctatetraene (cot), in which formally the newly formed P=N double bonds act as binding sites to the Ru^0 center. However, the long P–N bonds, which approach almost single-bond lengths (av 1.809(1) Å),[27] indicate very strong electron back donation, M→L, from the Ru center into the π*(p,p)-orbitals of the P=N bonds. This again leaves some ambiguity to the true oxidation state of the metal center and the ligand and complex **6** is likely best described by two resonance structures with a Ru^0 and a neutral 1,5,2,6-diazadiphosphocine ligand and one with a Ru^{II} center and a dianionic ligand. Two N-bound trop moieties coordinate with the $C{=}C_{trop}$ units and complete the coordination sphere around the Ru center, which resides in a distorted planar coordination sphere [ϕ 34.9°]. Also, the long $C{=}C_{trop}$ bonds (av 1.440(1) Å) indicate strong M→L π-electron back donation. The non-coordinated C31(33)–C32(34) (av 1.337(1) Å) and the newly formed P1(2)–C32(34) (av 1.847(1) Å) bonds show typical double and single-bond lengths, respectively.

2-Methyl-2-nitrosopropane MNP = *t*BuNO is a potent spin trap and is frequently used to probe radicals.[28] This blue nitroso reagent was generated by warming a benzene solution of the crystalline colorless dimer $[t\text{BuNO}]_2$ and collecting the monomer in THF at −78 °C containing complex **2×thf**. Upon warming to room temperature, the reaction mixture becomes immediately red, and an EPR-silent complex **7** is formed as the only spectroscopically observed species (Scheme 3). The structure was determined by X-ray diffraction methods and shows that *t*BuNO is bound to the metal center and not to the ligand (Figure 4A). The nitroso reagent *t*BuNO did not react as a radical trap in this experiment, but rather simply acts as N-donor ligand to bind to the ruthenium center, displacing the THF molecule in complex **2×thf** to form complex **7**. The Ru center resides in a distorted trigonal-bipyramidal coordination sphere (τ_5 0.57 vs. τ_5 0.10 in **2×thf**). The nitrone occupies the apical position in a common η^1-N coordination mode for this ligand. The plane of the nitroso ligand defined by the O1-N3-C bisects the angles between both centroids and the dad ligand nitrogen atoms, which seems to be the preferred orientation for steric reasons. The Ru–N3 bond length compares well with the Ru–N1/N2 distances (av 1.989(2) Å), and the N–O bond length (1.246(3) Å) indicates typical double-bond character.[29] The crystallographic parameters of the backbone indicate the 1,2-enediamide form [$^-$N-C=C-N$^-$].

When $Fe(CO)_5$ is reacted with **2×thf** in a 1.5:1 molar ratio, the diamagnetic heterobimetallic complex **8** is formed (Scheme 3). The CO displacement from the iron complex and transfer to the ruthenium is fast, and the reaction provides a striking example, in which both metal and ligand participate in the reaction. The ORTEP diagram of the molecular structure is shown in Figure 4B. The diazadiene ligand is bonded in a relatively rare σ-N,μ^2-N,η^2-C=N fashion,[30] in which two electrons

are donated by one σ-N iminic group (1.294(6) Å) to the Ru and four electrons through the other N=C group (1.413(7) Å) bridging the Ru and Fe atoms. Formally, the second iminic group donates two electrons through the bridging N atom and two electrons by η^2-bonding to the Fe center. The coordination sphere of the latter is completed by tree CO ligands and a Ru–Fe bond (2.744(1) Å). A pseudo-octahedral coordination sphere is formed around the ruthenium center with the largest deviation from the expected 90° bond angles for N1-Ru-N2 (81.1(2)°), relatively short $C{=}C_{trop}$ (1.449(6), 1.391(8) Å) and long Ru centroid bonds (2.060(5), 2.239(5) Å).

Computational studies

Calculated free-energy profile of nitrene insertion steps in the dad ligand

The pathway for conversion of **2** to **3**, involving activation of the azide, migration of the resulting ruthenium-bound imido moiety to the dad moiety of the $trop_2$dad ligand, and insertion of the nitrene into the C–C bond were explored with DFT at the closed-shell singlet (non-radical pathway), open-shell singlet, and triplet surfaces (radical pathways). The computations were performed at the b3-lyp, def2-TZVP level. To limit the computational costs, the calculations were performed by using a simplified representation of the $trop_2$dad ligand with each of the aromatic rings being replaced by -CH=CH-, and the adamantyl azide (AdN_3) substrate being replaced by methyl azide. On all spin surfaces considered, the reaction essentially follows the stepwise mechanism shown in Scheme 4: 1) Azide coordination to form intermediate **A**; 2) N_2 loss to form nitrene intermediate **B**; 3) Nitrene migration to one of the carbon atoms of the dad moiety to form intermediate **C**; 4) Formation of a second N–C bond to form "aziridine" intermediate **D**; and 5) "Aziridine" C–C bond cleavage to produce the final product **E**.

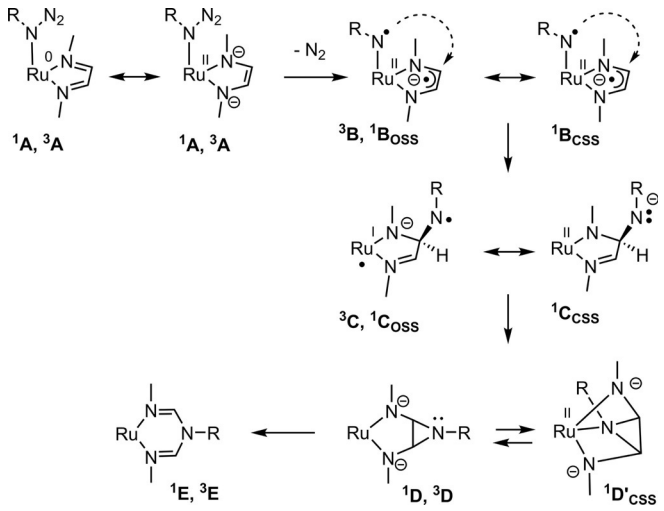

Scheme 4. Overview of the computed reaction steps converting **A**, via intermediates **B**, **C**, and **D**, into the final product **E** at three different spin configurations.

Singlet-triplet spin crossover phenomena may be operative (e.g., in the thermal equilibrium between ^{1}**D** and ^{3}**D**), but minimum-energy crossing points were not computed, because the computed triplet and singlet spin states are very close in energy (within a few kcal mol^{-1}) in all cases. Transitions between OSS and CSS singlet surfaces always proceed in a barrierless manner, because these are simply different DFT approximations of the same (singlet) state. The computed steps leading to conversion of **A** to **E** are discussed below in more detail.

Azide activation and migration of the nitrene moiety to the dad fragment

Elimination of dinitrogen from MeN_3 is the first step of the computed mechanism. The starting MeN_3 adduct **A** was calculated at the CSS and triplet spin surfaces (Scheme 5). No OSS solution was found. The computed barriers (**TS1**) for elimination of dinitrogen from **A** at the OSS and CSS surface are easily accessible at the experimentally applied reaction temperature, producing nitrene intermediates **B** (^{3}**B**, $^1\mathbf{B}_{oss}$, and $^1\mathbf{B}_{CSS}$).

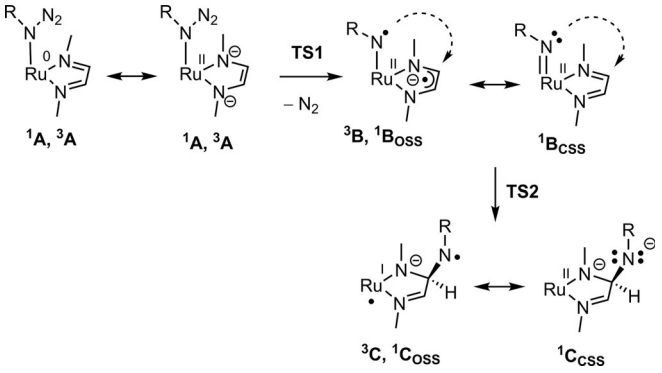

Scheme 5. Computed N_2 loss and nitrene transfer steps in the transformation of **A** to **C**.

The next step involves migration of the nitrene from the metal center to one of the carbon atoms of the dad moiety via **TS2**. As was computed for **TS1**, the lowest **TS2** barrier occurs at the OSS surface, but the CSS barrier is almost equally high (see Table 2). Nonetheless, the multireference character (OSS contribution) seems to be important in lowering the **TS1** and **TS2** barriers.

Intermediate **C** formed after nitrene migration to the dad moiety and is most stable in its triplet state. But the closed-shell singlet configuration of **C** is only slightly higher in energy.

Table 2. Computed free energies (ΔG°_{298K} in kcal mol^{-1}) for azide activation to produce intermediates **B**. Absolute energies relative to $^1\mathbf{A}_{CSS}$ (barriers within the singlet or triplet spin surface between brackets).

Spin conf.	A	TS1	B	TS2	C
CSS	0	+21.8 (+21.8)	−23.6	+1.8 (+25.4)	−15.4
OSS	–	+19.3 (+19.3)	−22.1	+1.0 (+24.6)	–
triplet	+3.4	+25.5 (+22.1)	−26.2	+6.5 (+32.7)	−16.6

No OSS solution of **C** was located. ^{1}**C** has a shorter Ru–N bond, which leads to a somewhat more strained geometry than for ^{3}**C**. The Ru–N_{dad} bonds of ^{3}**C** (1.99 Å; 2.07 Å) are significantly different than for ^{1}**C** (2.01 Å; 2.02 Å).

Subsequent transformations producing product E from intermediate C

The next step in the reaction sequence is a second N–C coupling step, converting intermediate **C** into "aziridine" intermediates ^{3}**D** or ^{1}**D′$_{CSS}$** (see Scheme 6). On the singlet surface, this process proceeds via ^{1}**TS3$_{CSS}$**, on the triplet surface via

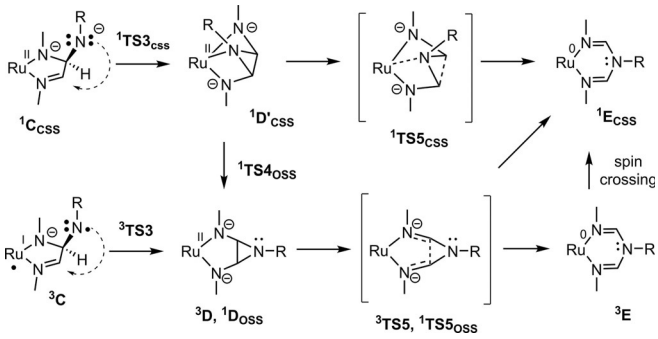

Scheme 6. Calculated reaction pathways for the conversion of intermediates ^{1}**C$_{CSS}$** or ^{3}**C** to the final product ^{1}**E$_{CSS}$**.

^{3}**TS3**, and both surfaces lie very close in energy. No OSS solutions were located for **C** or **TS3** in this step. The Ru–N interactions are quite different at the triplet and singlet surfaces. Although in ^{1}**TS3 c$_{ss}$** the "aziridine" nitrogen is closely interacting with Ru (2.07 Å), the corresponding Ru–N distance in ^{3}**TS3** is at non-bonding distance (3.33 Å). The same is true for the resulting products ^{3}**D** and ^{1}**D′$_{CSS}$**. Although in ^{3}**D** the "aziridine" nitrogen is completely separated from Ru (3.19 Å), it has a short Ru–N distance (2.10 Å) in ^{1}**D′$_{CSS}$**. The intermediate ^{1}**D′$_{CSS}$** is only 1.8 kcal mol^{-1} less stable than ^{3}**D**. ^{1}**TS4$_{OSS}$** directly connects ^{1}**D′$_{CSS}$** and ^{1}**D$_{OSS}$** in a thermal equilibrium reaction at the (open-shell) singlet surface. Interconversion of OSS species ^{1}**D$_{OSS}$** and triplet species ^{3}**D** in a thermal equilibrium reaction requires spin crossover. We did not explore the MECP of this process though, in view of the very small energy difference between these species.

In the next step, the aziridine moiety in ^{1}**D′$_{CSS}$** or ^{3}**D** needs to rearrange such that the final product **E** is obtained. On the closed-shell singlet energy surface one pathway was found, which converts isomer ^{1}**D′$_{CSS}$** through the activated complex ^{1}**TS5$_{CSS}$** (barrier: +11.8 kcal mol^{-1}) directly to **E**. On the triplet surface, isomer ^{3}**D** with a non-coordinated aziridine ring is transformed via ^{3}**TS5** (barrier: +2.0 kcal mol^{-1}) to the final product ^{3}**E** (Scheme 6, Table 3). The barrier via ^{3}**TS5** is lower than via ^{1}**TS5$_{CSS}$**, which we assume is due to the fact that in ^{1}**TS5$_{CSS}$** not only the C–C bond, but also the Ru–N bond must be broken. In ^{3}**D** and ^{3}**TS5**, the aziridine moiety does not interact with Ru, and only the bridging C–C bond must be broken. The final product is 18 kcal mol^{-1} more stable in its singlet configuration ^{1}**E** than the one in triplet configuration ^{3}**E**. Hence, if the reaction would proceed over the triplet surface, a final spin-crossing step must occur to form ^{1}**E**. But an alternative pathway over low-energy barriers is available on the singlet surface. This proceeds from ^{1}**D′$_{CSS}$** through an activated complex ^{1}**TS4$_{OSS}$** (barrier: +6.7 kcal mol^{-1}) with an open-shell singlet configuration (see Scheme 6). This produces ^{1}**D$_{OSS}$**, which—as in triplet ^{3}**D**, but in contrast to ^{1}**D′**—has no $N_{aziridine}$–Ru bond. Subsequent cleavage of the bridging aziridine C–C bond via the activated complex ^{1}**TS5$_{OSS}$** is nearly barrierless and produces ^{1}**E** with a closed-shell singlet (CSS) configuration directly. Hence, while dissociation of the aziridine nitrogen atom and breaking of the bridging aziridine C–C bond occur simultaneously in ^{1}**TS5$_{CSS}$**, the two processes are decoupled for the process ^{1}**D′$_{CSS}$** to ^{1}**E** via ^{1}**TS4$_{OSS}$** and ^{1}**TS5$_{OSS}$** on the OSS pathway (Table 3).

Table 3. Computed free energies (ΔG°_{298K} in kcal mol^{-1}) for subsequent transformation producing product **E** from intermediate **C** at the different spin surfaces. Absolute energies relative to ^{1}**A$_{CSS}$** (relative barriers within the singlet or triplet spin surface between brackets).

Spin conf.	C	TS3	D′$_{CSS}$	TS4$_{OSS}$	D	TS5	E
CSS	−15.4	−5.6 (+9.8)	−10.1	–	–	+1.7 (+11.8)	−64.7
OSS	–	–	–	−3.4 (+6.7)	−9.7	−9.2 (+0.5)	–
triplet	−16.6	−6.8 (+9.8)	–	–	−11.9	−9.9 (+2.0)	−47.2

The computed pathways along the CSS, OSS, and triplet surface all proceed via accessible reaction barriers for all steps considered. Considering the small-energy differences, reliable distinction between the reaction paths proceeding at different spin surfaces is not possible on the basis of DFT. As such, we refrain from discriminating between these pathways, and hence both radical- and non-radical reaction steps could be operative. However, in any case, the multireference character (open-shell singlet contribution) seems to be important in lowering some of the singlet state transition state barriers (**TS1**, **TS2**, and **TS5**).

Calculated free-energy profile of carbene insertion in the C–C bond of the dad ligand

The computed pathway for carbene insertion into the dad C–C bond of **2×thf** to form the ligand-protonated form of complex **4** (i.e., complex **F-c** in Scheme 7) is qualitatively similar to the nitrene insertion pathway discussed above. Elimination of dinitrogen from diazomethane (CH_2N_2) is the first step of the computed mechanism, which occurs with a relatively low barrier of +6 kcal mol^{-1}. This is followed by transfer of the carbene moiety to the dad fragment, which occurs via a two-step process involving electrophilic addition of CH_2 moiety to the dad π system, followed by (homolytic) splitting of the Ru–C bond. The next steps in the reaction pathway involve a second C–C coupling followed by cleavage of the C–C bond stemming

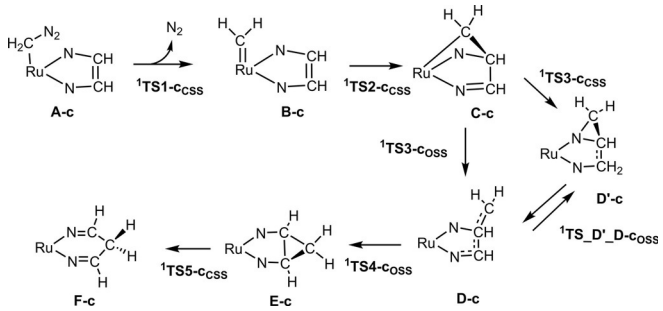

Scheme 7. Computed pathway for diazomethane activation and carbene insertion into the dad framework.

from the dad moiety producing complex **F-c**. This process proceeds via a low barrier at TS5-CSS. From here on a base-assisted pathway leads to formation of **5** via complex **4**. Formation of complex **5** by water-assisted proton transfer to the metal center in intermediate **F-c** is also possible, and has a computed transition state barrier of $+18.2$ kcal mol^{-1}. Interestingly, for the carbene insertion reaction, DFT points to divergent pathways at the OSS and CSS surface, with the lower-barrier steps of the radical-type OSS pathway being substantially different from the two-electron steps along the CSS path (Scheme 7 and Figure S42 in the Supporting Information). Therefore, these insertion reactions provide a rare example, in which a singlet-diradical reacts differently from its closed-shell counterpart (see the Supporting Information for details).

Conclusions

The present study reveals the unusual reactivity of the [Ru(trop$_2$dad)(thf)] (**2×thf**) complex towards a series of electrophilic substrates, mostly resulting in ligand-centered transformations. DFT studies revealed that the closed-shell singlet (CSS), open-shell singlet (OSS), and triplet electronic structures of the complex are close in energy, with the open-shell singlet configuration being lowest in energy. Although a reliable discrimination between these spin configurations with DFT is impossible, the OSS and triplet ruthenium(I)–dad ligand radical configurations do seem to have an important contribution to the electronic structure and reactivity of **2×thf**. Several ligand-based reactions were disclosed. Particularly notable are the reactions with AdN_3 and diazomethane, resulting in net (formal) nitrene and carbene insertion in the C–C bond of the dad ligand moiety, respectively. DFT calculations revealed pathways with lower energy barriers for the OSS and triplet radical-type pathways compared to the non-radical closed-shell trails leading to these products. The combined DFT data further suggest that the dad$^{\bullet-}$ ligand radical character of the ruthenium species described in this paper is of importance to understand their intrinsic reactivity, because several of the computed CSS transition-state barriers proved to be substantially higher than the OSS and/or triplet transition-state barriers. The complex further reacts with the silyl-substituted phosphaalkyne Ph_3SiCP to undergo a cycloaddition producing an unprecedented heterocyclic structure. The nitroso compound *t*BuNO only binds to Ru as an N ligand, whereas a metal carbonyl adds to both the metal and the dad ligand. These preliminary results may have an impact on the further development and better understanding of reactivity patterns of complexes with redox non innocent and cooperative ligands. They also stress the importance of considering different spin surfaces in (computed) reaction mechanisms.

Acknowledgements

This work was supported by the Schweizer Nationalfonds (SNF), Eidgenössische Technische Hochschule Zürich, the Netherlands Organization for Scientific Research NWO-CW (VICI project 016.122.613), the FOM-NWO-Shell Computational Sciences for Energy Research Initiative (project 13CSER003), and the RPA Sustainable Chemistry of the University of Amsterdam. V.S. carried out computational study, guided by B.dB. V.S. and B.dB. thank the ORCA forum and the ORCA team, specially Mr. Kanthen Sivalingam and Dr. Shengfa Ye, for helpful discussions regarding CASSCF calculations. V.S. thanks Dr. Simon Mathew for help with extra computer time. All authors discussed the results and wrote the manuscript together.

Conflict of interest

The authors declare no conflict of interest.

Keywords: azides · olefin ligands · redox chemistry · ruthenium · synthetic methods

[1] H. Grützmacher, *Angew. Chem. Int. Ed.* **2008**, *47*, 1814; *Angew. Chem.* **2008**, *120*, 1838.
[2] a) H. B. Gray, E. Billig, *J. Am. Chem. Soc.* **1963**, *85*, 2019; b) A. Davison, N. Edelstein, R. H. Holm, A. H. Maki, *J. Am. Chem. Soc.* **1963**, *85*, 2029; c) C. K. Jørgensen, *Coord. Chem. Rev.* **1966**, *1*, 164; d) K. G. Caulton, *Eur. J. Inorg. Chem.* **2012**, 435.
[3] a) V. Lyaskovskyy, B. de Bruin, *ACS Catal.* **2012**, *2*, 270; b) O. R. Luca, R. H. Crabtree, *Chem. Soc. Rev.* **2013**, *42*, 1440; c) D. G. H. Hetterscheid, A. Koekkoek, H. Grützmacher, B. de Bruin, *Prog. Inorg. Chem.* **2007**, *55*, 249; d) P. Chirik, K. Wieghardt, *Science* **2010**, *327*, 794; e) *Cooperating Ligands in Catalysis, M. Trincado, H. Grützmacher, in Cooperative Catalysis* (Ed.: R. Peters), Wiley-VCH, Weinheim, **2014**, pp. 67 – 111; f) M. Trincado, D. Banerjee, H. Grützmacher, *Energy Environmental Science* **2014**, *7*, 2464.
[4] W. Kaim, B. Schwederski, *Coord. Chem. Rev.* **2010**, *254*, 1580.
[5] See for example: M. G. Scheibel, B. Askevold, F. W. Heinemann, E. J. Reijerse, B. de Bruin, S. Schneider, *Nat. Chem.* **2012**, *4*, 552.
[6] See, for example: a) H. Tsurugi, T. Saito, H. Tanahashi, J. Arnold, K. Mashima, *J. Am. Chem. Soc.* **2011**, *133*, 18673; b) For a review, see: G. van Koten, K. Vrieze, *Adv. Organomet. Chem.* **1982**, *21*, 151.
[7] S. Berger, F. Baumann, T. Scheiring, W. Kaim, *Z. Anorg. Allg. Chem.* **2001**, *627*, 620.
[8] a) F. F. Puschmann, J. Harmer, D. Stein, H. Rüegger, B. de Bruin, H. Grützmacher, *Angew. Chem. Int. Ed.* **2010**, *49*, 385; *Angew. Chem.* **2010**, *122*, 395; b) T. Bally, *Nat. Chem.* **2010**, *2*, 165.
[9] R. E. Rodríguez-Lugo, M. Trincado, M. Vogt, F. Tewes, G. Santiso-Quinones, H. Grützmacher, *Nat. Chem.* **2013**, *5*, 342.
[10] M. Trincado, V. Sinha, R. E. Rodriguez-Lugo, B. Pribanic, B. de Bruin, H. Grützmacher, *Nat. Commun.* **2017**, *8*, 14990.
[11] The τ_5 values of 0 and 1 indicate perfect square-pyramidal and trigonal-bipyramidal geometries, respectively. A. W. Addison, T. N. Rao, J. Reedijk, J. van Rijn, G. C. Verschoor, *J. Chem. Soc. Dalton Trans.* **1984**, 1349.

[12] C. Lichtenberg, M. Adelhardt, T. Gianetti, K. Meyer, B. de Bruin, H. Grützmacher, *ACS Catal.* **2015**, *5*, 6230.
[13] C. Lichtenberg, L. Viciu, M. Vogt, R. E. Rodriguez-Lugo, M. Adelhardt, J. Sutter, M. M. Khusniyarov, K. Meyer, B. de Bruin, E. Bill, H. Grützmacher, *Chem. Commun.* **2015**, *51*, 13890.
[14] a) Geometries were optimized with Turbomole at the DFT-D3, hybrid b3-lyp, def2-TZVP level, employing Grimme's version 3 dispersion corrections. b) CASSCF-NEVPT2 calculations were performed using the ORCA suit of programs, applying the def2-TZVP basis set. See the Supporting Information for more details concerning the applied methods and programs.
[15] P. H. M. Budzelaar, B. de Bruin, A. W. Gal, K. E. Wieghardt, J. H. van Lenthe, *Inorg. Chem.* **2001**, *40*, 4649.
[16] a) T. Zell, P. Milko, K. L. Fillman, Y. Diskin-Posner, T. Bendikov, M. A. Iron, G. Leitus, Y. Ben-David, M. L. Neidig, D. Milstein, *Chem. Eur. J.* **2014**, *20*, 4403; b) B. Butschke, K. L. Fillman, T. Bendikov, L. J. W. Shimon, Y. Diskin-Posner, G. Leitus, S. I. Gorelsky, M. L. Neidig, D. Milstein, *Inorg. Chem.* **2015**, *54*, 4909.
[17] Other transition metal, with exception of ruthenium, containing a planar M-N-C-N-C-N metallocycle are known: a) V. Robinson, G. E. Taylor, P. Woodward, M. I. Bruce, R. C. Wallis, *J. Chem. Soc. Dalton Trans.* **1981**, 1169; b) W. J. Bland, R. D. Kemmitt, I. W. Nowell, R. D. Russell, *Chem. Commun.* **1968**, 1065; c) M. Bonamico, V. Fares, A. Flamini, P. Imperatori, N. Poli, *Angew. Chem. Int. Ed.* **1989**, *28*, 1049; *Angew. Chem.* **1989**, *101*, 1067; d) J. D. Masuda, D. W. Stephan, *Can. J. Chem.* **2005**, *83*, 477.
[18] Insertion of a nitrene moiety in a diazadiene ligand has been observed once before: S. P. Heins, W. D. Morris, P. T. Wolczanski, E. B. Lobkovsky, T. R. Cundari, *Angew. Chem. Int. Ed.* **2015**, *54*, 14407; *Angew. Chem.* **2015**, *127*, 14615.
[19] For an example of a stable ruthenium methylene complex formed by reaction of diazomethane with a coordinatively unsaturated Ru^{II} complex, see: D. S. Bohle, G. R. Clark, C. E. F. Rickard, W. R. Roper, W. E. B. Shepard, L. J. Wright, *J. Chem. Soc. Chem. Commun.* **1987**, 563.
[20] B. Morandi, E. M. Carreira, *Science* **2012**, *335*, 1471.
[21] For a reviews of metal β-diketiminates, see: a) L. Bourget Merle, M. F. Lappert, J. R. Severn, *Chem. Rev.* **2002**, *102*, 3031; b) Y. C. Tsai, *Coord. Chem. Rev.* **2012**, *256*, 722.
[22] Previously reported examples of Ru-NacNac complexes exhibit similar metric parameters: a) A. D. Phillips, O. Zava, R. Scopelitti, A. A. Nazarov, P. J. Dyson, *Organometallics* **2010**, *29*, 417; b) A. D. Phillips, K. Thommes, R. Scopelliti, C. Gandolfi, M. Albrecht, K. Severin, D. F. Schreiber, P. J. Dyson, *Organometallics* **2011**, *30*, 6119.
[23] For examples of cyclodimerization of phosphaalkynes, see: a) P. B. Hitchcock, M. J. Maah, J. F. Nixon, *J. Chem. Soc. Chem. Commun.* **1986**, 737; b) P. Binger, R. Milczarek, R. Mynott, C. Krüger, Y.-H. Tsay, E. Raabe, M. Regitz, *Chem. Ber.* **1988**, *121*, 637; c) T. Wettling, G. Wolmershäuser, P. Binger, M. Regitz, *J. Chem. Soc. Chem. Commun.* **1990**, 1541; d) M. Driess, D. Hu, H. Pritzkow, H. Schäufele, U. Zenneck, M. Regitz, W. Rösch, *J. Organomet. Chem.* **1987**, *334*, C35; e) P. Binger, B. Biedenbach, R. Schneider, M. Regitz, *Synthesis* **1989**, 960; f) For examples of trimerization, see: R. Milczarek, W. Rüssler, P. Binger, K. Jonas, K. Angermund, C. Krüger, M. Regitz, *Angew. Chem. Int. Ed. Engl.* **1987**, *26*, 908; *Angew. Chem.* **1987**, *99*, 957; g) M. Trincado, A. J. Rosenthal, M. Vogt, H. Grützmacher, *Eur. J. Inorg. Chem.* **2014**, 1599.
[24] W. Rösch, M. Regitz, *Angew. Chem. Int. Ed. Engl.* **1984**, *23*, 900; *Angew. Chem.* **1984**, *96*, 898.
[25] a) J. G. Cordaro, D. Stein, H. Rüegger, H. Grützmacher, *Angew. Chem. Int. Ed.* **2006**, *45*, 6159; *Angew. Chem.* **2006**, *118*, 6305; b) For a more recent study on coordination chemistry of trimethylsilylphosphaalkyne, see: S. M. Mansell, M. Greena, C. A. Russella, *Dalton Trans.* **2012**, *41*, 14360.
[26] Only 1,5,3,7-diazadiphosphocine heterocycles have been described previously in the literature, mainly as diphosphine ligands coordinated to late transition metals, with two pendant cooperative amines. See, for example: T. Liu, D. L. DuBois, R. M. Bullock, R. Morris, *Nat. Chem.* **2013**, *5*, 228.
[27] G. Trinquier, M. T. Ashby, *Inorg. Chem.* **1994**, *33*, 1306.
[28] A. Alberti, M. Guerra, A. Venturini, *RSC Adv.* **2013**, *3*, 17887.
[29] S. F. Palopoli, S. J. Geib, A. L. Reingold, T. B. Brill, *Inorg. Chem.* **1988**, *27*, 2963.
[30] There are only few complexes containing diazadiene as 6e donor ligands, see for example: H. W. Frühauf, A. Landers, R. Goddard, C. Krueger, *Angew. Chem. Int. Ed. Engl.* **1978**, *17*, 64; *Angew. Chem.* **1978**, *90*, 56.

Manuscript received: December 15, 2017
Accepted manuscript online: January 17, 2018
Version of record online: February 27, 2018

